

The Rapid Growth and Decay of an Extratropical Cyclone over the Central Pacific Ocean

JONATHAN E. MARTIN

Department of Atmospheric and Oceanic Sciences, University of Wisconsin—Madison, Madison, Wisconsin

JASON A. OTKIN

Cooperative Institute for Meteorological Satellite Studies, Space Science and Engineering Center, University of Wisconsin—Madison, Madison, Wisconsin

(Manuscript received 22 April 2003, in final form 6 November 2003)

ABSTRACT

The life cycle of a central Pacific cyclone, characterized by a 48-h interval of rapid fluctuation in its intensity, is examined. The cyclone of interest underwent a period of explosive cyclogenesis from 1200 UTC 4 November to 1200 UTC 5 November 1986, followed 12 h later by a period of unusually rapid decay. Output from a numerical simulation of this event, run using the fifth-generation Pennsylvania State University–National Center for Atmospheric Research (PSU–NCAR) Mesoscale Model (MM5), is used to perform a piecewise potential vorticity (PV) inversion in order to diagnose the life cycle of this unusual cyclone.

The analysis reveals that the presence of lower-tropospheric frontogenetic forcing in an environment characterized by reduced static stability (as measured by high values of the K index) produced a burst of heavy precipitation during the development stage of the cyclone's life cycle. The associated latent heat release produced a substantial diabatic PV anomaly in the middle troposphere that was, in turn, responsible for the majority of the lower-tropospheric height falls associated with the explosive cyclogenesis. Subsequent height rises during the rapid cyclolysis stage resulted from the northward migration of the surface cyclone into a perturbation geopotential ridge associated with a negative tropopause-level PV anomaly. This feature developed rapidly in response to the southeastward migration of a preexisting, upstream negative PV anomaly and the production of a second negative tropopause-level PV anomaly to the north of the surface cyclone. This latter feature was a diabatic consequence of the latent heat release that fueled the explosive development. Thus, the very latent heat release that assisted in the rapid development of the cyclone also played an important role in its subsequent decay. It is suggested that such a life cycle may represent an example of a "self-destroying" system.

1. Introduction

The typical extratropical cyclone life cycle lasts about 5 days and consists of an extended period of moderate development followed by an extended period of gradual decay. A small percentage of these cyclones experience a period of extremely rapid development during which the sea level pressure (SLP) minimum at the cyclone center falls at a rate exceeding 1 hPa h^{-1} for at least 24 h^1 (Sanders and Gyakum 1980). The physical characteristics of these "bombs," as well as

their geographical distribution, has been the subject of considerable research during the last quarter century (e.g., Sanders and Gyakum 1980; Roebber 1984; Sanders 1986; Colucci and Alberta 1996; Sinclair 1997; Sinclair and Revell 2000). In their pioneering study of explosive cyclogenesis, Sanders and Gyakum (1980) noted that the frequency of occurrence of such storms bore a close relationship to the warm Kurishio and Gulf Stream currents in the Northern Hemisphere (see Fig. 3 of Sanders and Gyakum 1980). In a subsequent statistical analysis, Roebber (1984) noted that cyclones that experience a period of rapid deepening are also likely to experience a longer period of development than less intense, "ordinary" storms. Most case studies of rapid cyclogenesis events have examined cyclones that developed along the western boundary currents (e.g., Anthes et al. 1983; Kuo and Reed 1988; Whitaker et al. 1988; Manobianco 1989; Kuo et al. 1991; Bosart et al. 1995), while very few, if any, case studies of

¹ Sanders and Gyakum (1980) define this threshold rate by multiplying the observed pressure tendency by $(\sin 60^\circ / \sin \phi)$ where ϕ is latitude.

Corresponding author address: Dr. Jonathan E. Martin, Dept. of Atmospheric and Oceanic Sciences, University of Wisconsin—Madison, 1225 W. Dayton St., Madison, WI 53706.
E-mail: jon@aos.wisc.edu

rapid cyclogenesis in the central Pacific Ocean have been undertaken.²

Though the decay phase of the extratropical cyclone life cycle is often gradual, a small subset of cyclones experience fairly rapid cyclolysis. These storms have recently been examined from the synoptic-climatological, case study, and local energetics perspectives (Martin et al. 2001; Martin and Marsili 2002; McLay and Martin 2002). In a comprehensive 11-yr synoptic climatology of North Pacific cyclones, Martin et al. (2001) found that the frequency maxima of rapid cyclolysis events occur near the end of the Pacific storm track within the Bering Sea and Gulf of Alaska regions. Very few cases of abrupt surface cyclolysis were found to occur south of 45°N and virtually none occurred in the central Pacific (see Figs. 9 and 11 of Martin et al. 2001).

In this paper, the life cycle of an unusual central Pacific cyclone is examined. This storm was characterized by a 48-h interval of rapid fluctuation in its intensity, which included a period of explosive cyclogenesis followed 12 h later by a period of unusually rapid decay. Output from a successful numerical simulation³ of this event run using the fifth-generation Pennsylvania State University–National Center for Atmospheric Research (PSU–NCAR) Mesoscale Model (MM5) is used to perform a piecewise potential vorticity (PV) inversion in order to determine the relative roles of upper-tropospheric, lower-tropospheric, and diabatic processes in the rapid growth and decay of this cyclone. The paper is organized as follows. Section 2 provides a synoptic overview of the case using analyses from the European Centre for Medium-Range Weather Forecasts Tropical Ocean Global Atmosphere (ECMWF TOGA) dataset. In section 3 the model simulation will be described and compared to the analyses presented in section 2. An analysis of the model output from a piecewise PV inversion perspective is presented in section 4. Further investigation of the influence of latent heat release on the cyclone structure and life cycle is offered in section 5. Discussion and conclusions are given in section 6.

2. Synoptic overview

The scarcity of standard observational data in the central Pacific Ocean compels the use of an analysis product as a proxy for the observations in this region. We chose to use the ECMWF TOGA analyses in our investigation. This dataset consists of twice-daily SLP and standard pressure level analyses (1000, 850, 700, 500, 400, 300, 250, 200, 150, 100, and 50 hPa) on a

global domain with $2.5^\circ \times 2.5^\circ$ horizontal resolution. We begin the synoptic overview at 0000 UTC 5 November 1986.

a. 0000 UTC 5 November 1986

At 1200 UTC 4 November 1986 an SLP minimum of 1014 hPa was located west of Hawaii near 27°N, 172°W (not shown). By 0000 UTC 5 November that weak disturbance had moved northeastward to near 31°N, 167°W and developed into a surface cyclone (hereafter referred to as the primary cyclone) of modest intensity with an SLP minimum of 1002 hPa (Fig. 1a). The primary cyclone was straddled by prominent anticyclones characterized by SLP maxima exceeding 1032 hPa. Far to the north, a second cyclone, with an SLP minimum of 1006 hPa, was located along the eastern end of the Aleutian Islands chain. At this time the primary cyclone was associated with a neutrally tilted, upper-tropospheric wave that was characterized by sharp curvature in the 300-hPa flow (Fig. 1b). Hoskins et al. (1978) showed that convergence of the \mathbf{Q} vector identifies regions of quasigeostrophic forcing for ascent. The 500–700-hPa column-averaged \mathbf{Q} vectors and \mathbf{Q} -vector convergence attest to the potency of this upper-tropospheric wave in affecting lower- to middle-tropospheric ascent and associated surface cyclogenesis (Fig. 1c). Finally, the isolated nature of the upper wave perturbation is demonstrated by the 250–300-hPa column-averaged PV, which indicates that a tropopause PV maximum was located in the subtropical central Pacific flanked by low PV to its east and west (Fig. 1d).

b. 1200 UTC 5 November 1986

By 1200 UTC 5 November, the primary cyclone had moved nearly straight northward to 34°N, 172°W and deepened an impressive 21 hPa to 981 hPa (Fig. 2a). This explosive development period was coincident with an intensification of the SLP maximum to the east and a weakening of the SLP maximum to the west. At 300 hPa the development of a pronounced ridge on the downstream side of the trough axis (often the signature of considerable latent heat release) had subtly changed the shape of the upper wave. Also, the ridge axis to the west of the trough had become more positively tilted, as it continued to progress eastward (Fig. 2b). During this period of explosive development, the 500–700-hPa column-averaged \mathbf{Q} -vector convergence directly above the surface cyclone had strengthened and was now aligned into a north–south couplet (Fig. 2c) as opposed to the east–west couplet visible at 0000 UTC 5 November (Fig. 1c). Dramatic changes also occurred near the tropopause as the 250–300-hPa column-averaged PV filament evident 12 h earlier had significantly wrapped up at its southern end by this time (Fig. 2d). The treble clef shape of this PV feature is suggestive of an occluded thermal structure in the underlying troposphere (Martin

² The case of rapid cyclogenesis examined by Reed and Albright (1986) began to deepen rapidly east of 155°W and experienced its most rapid deepening east of 143°W and so is best characterized as eastern Pacific cyclogenesis.

³ “Successful” is defined as reasonable agreement between the simulation’s depiction of the sea level pressure, geopotential height, thermal structure, and upper-tropospheric PV structure as compared to that of the analyses.

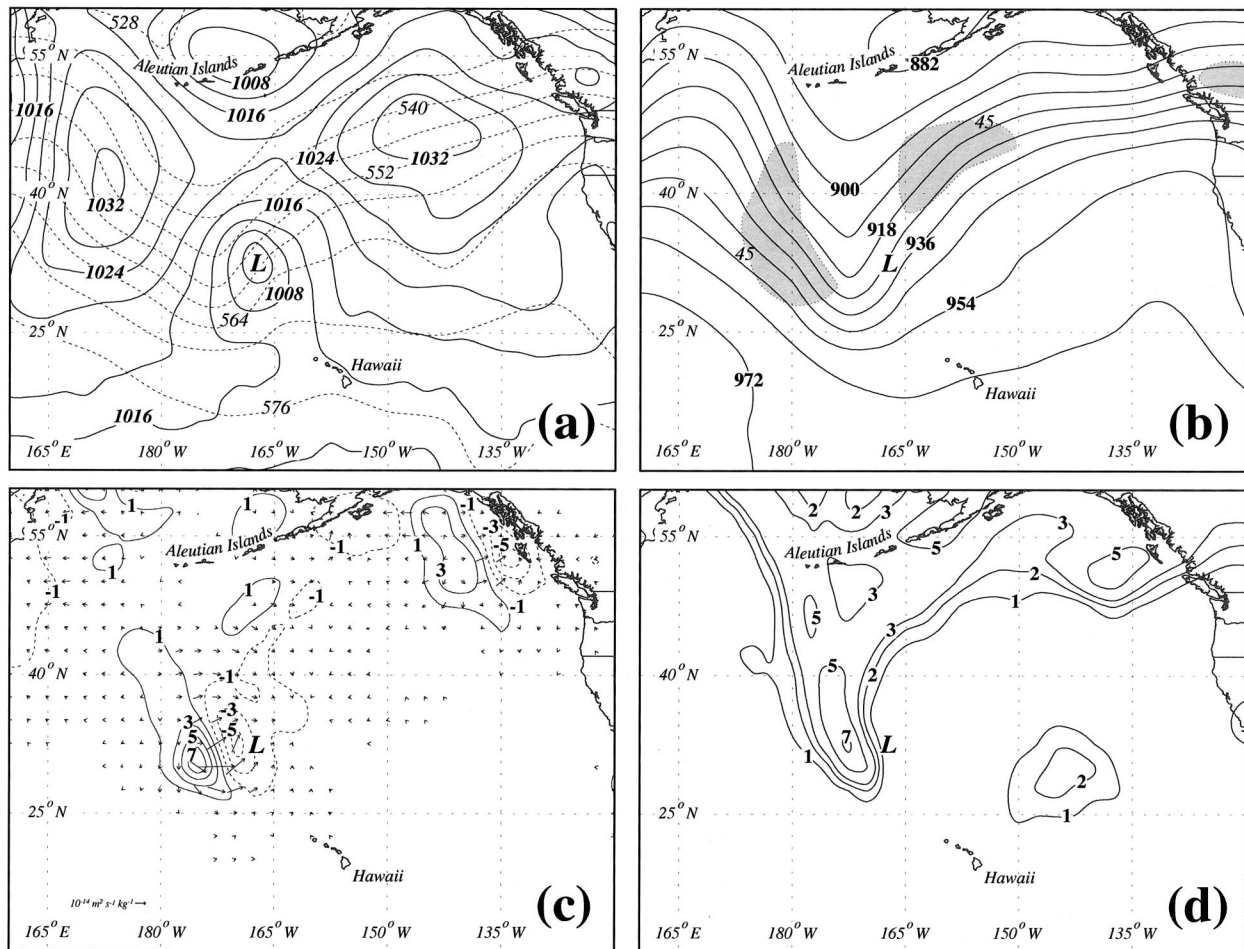


FIG. 1. (a) ECMWF analyses of SLP (solid lines) and 1000–500-hPa thickness (dashed lines) valid at 0000 UTC 5 Nov 1986. Sea level pressure labeled in hPa and contoured every 4 hPa. Thickness labeled in dam and contoured every 6 dam. The L (in each panel) represents the location of the SLP minimum. (b) ECMWF analyses of 300-hPa geopotential height (solid lines) and isotachs valid at 0000 UTC 5 Nov 1986. Geopotential height is labeled in dam and contoured every 9 dam while isotachs are labeled in m s^{-1} and shaded every 10 m s^{-1} beginning at 45 m s^{-1} . (c) ECMWF analyses of 500–700-hPa column-averaged \mathbf{Q} vectors and \mathbf{Q} -vector divergence valid at 0000 UTC 5 Nov 1986. The \mathbf{Q} -vector divergence is labeled in units of $10^{-15} \text{ m}^2 \text{ s}^{-1} \text{ kg}^{-1}$ and contoured every $2 \times 10^{-15} \text{ m}^2 \text{ s}^{-1} \text{ kg}^{-1}$ beginning at $1 (-1) \times 10^{-15} \text{ m}^2 \text{ s}^{-1} \text{ kg}^{-1}$. (d) ECMWF analysis of 250–300-hPa column-averaged potential vorticity labeled in PVU ($10^{-6} \text{ m}^2 \text{ K kg}^{-1} \text{ s}^{-1}$) and contoured every 1 PVU.

1998) and indeed such a structure in the 1000–500-hPa thickness field is evident at this time (Fig. 2a). Also notable is the sharp tropopause PV gradient on the eastern edge of the PV filament (roughly parallel to the Aleutian Islands).

c. 0000 UTC 6 November 1986

During the 12-h period ending at 0000 UTC 6 November, the primary cyclone experienced no change in intensity as it continued its northward movement (Fig. 3a). Note that the downstream anticyclone had further intensified to 1041 hPa by this time. This intensification was coincident with the continued growth of the upper-tropospheric ridge south of the Aleutian Islands (Fig. 3b).

At 300 hPa the upper wave associated with the surface cyclone had become cutoff to the south of a region of nearly continuous, anticyclonically curved flow extending from west of the date line to the Pacific Northwest (Fig. 3b). The 500–700-hPa column-averaged \mathbf{Q} -vector convergence maximum was located downshear (in a thermal wind sense) of the surface low and had dramatically weakened, reflecting a diminution of synoptic-scale forcing for ascent in the vicinity of the surface cyclone (Fig. 3c). A substantial change in the tropopause-level PV structure also occurred during this period. What had been a treble clef-shaped PV filament 12 h earlier had become elongated and weakened by 0000 UTC 6 November (Fig. 3d). Also, the low-PV air east of the filament had moved farther north by this time.

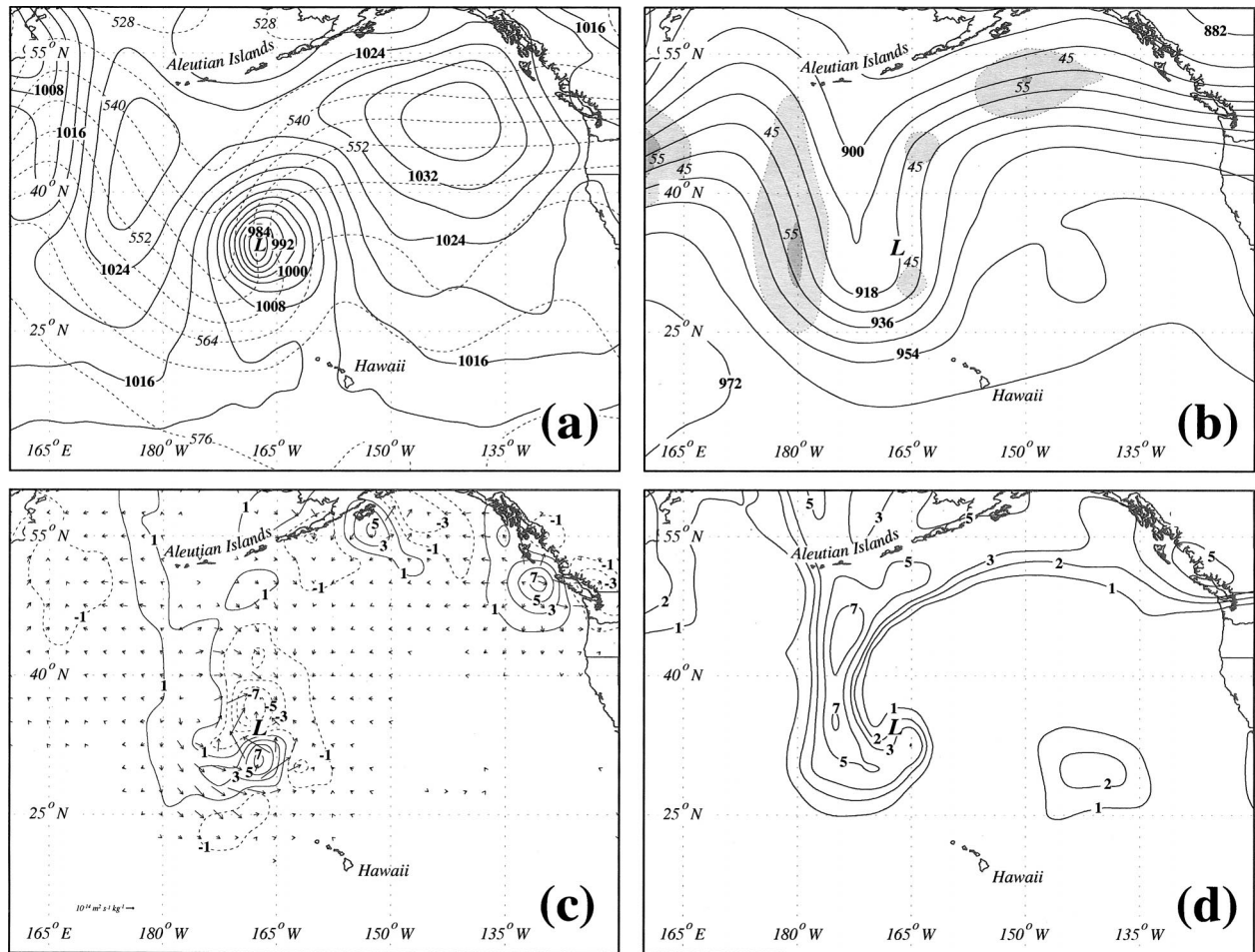


FIG. 2. As for Fig. 1 except from the ECMWF analyses valid at 1200 UTC 5 Nov 1986.

d. 1200 UTC 6 November 1986

The SLP minimum associated with the primary cyclone filled by 10 hPa to 991 hPa during the 12-h period ending at 1200 UTC 6 November (Fig. 4a). This rate of SLP increase, while falling just shy of the value of 12 hPa 12 h^{-1} set by Martin et al. (2001) in their definition of rapid surface cyclolysis, nevertheless places this cyclone in the 88th percentile in its rapidity of decay as compared to all other Pacific storms and it decayed much farther south than those in the climatology. At 300 hPa there had also been a significant height rise at the center of the primary upper trough during this 12-h period as the cutoff cyclone visible 12 h earlier had eroded by 1200 UTC (Fig. 4b). The anticyclonic curvature of the flow north of the equatorward-protruding primary trough had intensified during this 12-h period as well. Note that the base of the primary upper trough had made steady progress toward Hawaii during its entire 36-h evolution. The 500–700-hPa column-averaged \mathbf{Q} -vector convergence displayed a weakened couplet in the vicinity of the primary cyclone (Fig. 4c) testifying

to the lack of synoptic-scale support for cyclogenesis by this time. The tropopause PV feature had become further isolated while the low-PV air in the 250–300-hPa layer continued to expand to the north and east, roughly mirroring the coastline of the Pacific Northwest by this time (Fig. 4d). During this 36-h evolution the primary PV feature had raced southward, undergone a short-lived period of cyclonic wrapup, and then abruptly become cutoff, stretched, and diluted. Some of these latter elements also characterized the behavior of the tropopause PV associated with the case of rapid cyclolysis diagnosed by Martin and Marsili (2002).

3. Model description and evaluation

In order to identify the physical mechanisms responsible for the rapid fluctuation in intensity experienced by the primary cyclone, gridded output from a successful numerical simulation of the event, performed using version 3 of the PSU–NCAR MM5 modeling system (Grell et al. 1994), was used. The model simulation

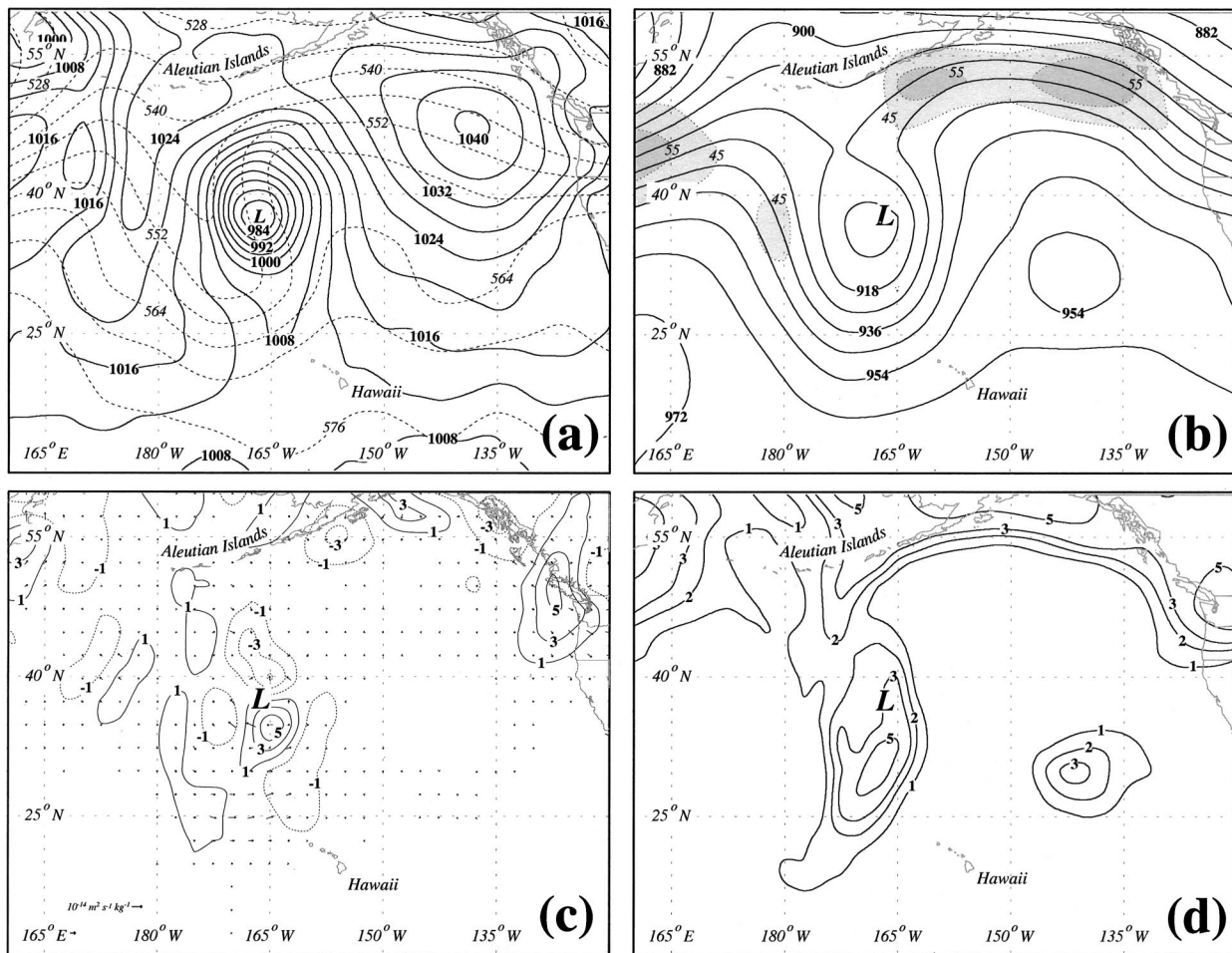
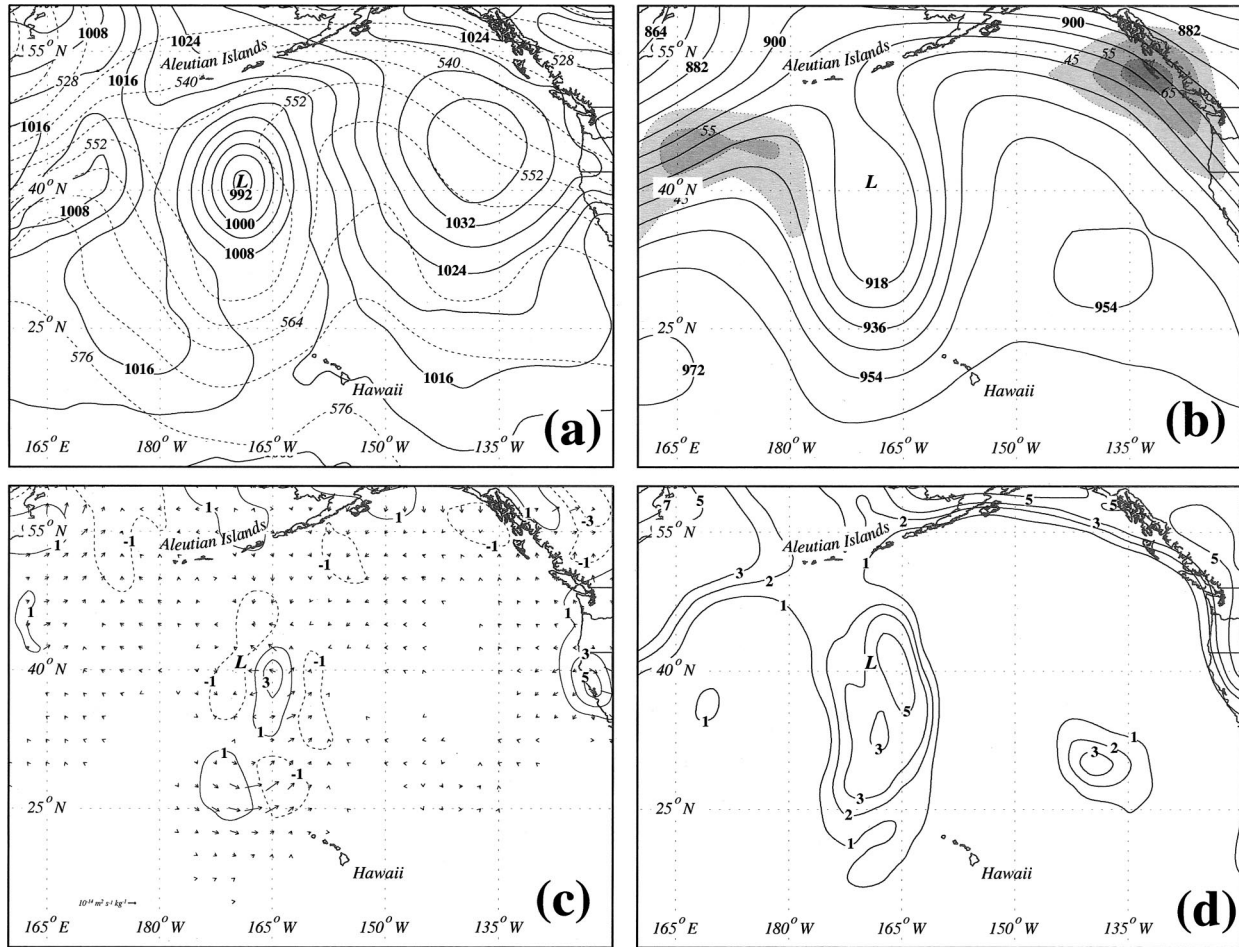


FIG. 3. As for Fig. 1 except from the ECMWF analyses valid at 0000 UTC 6 Nov 1986.

employs a one-way nested grid with a coarse outer domain (grid 1) and a finer-scale inner domain (grid 2) with horizontal grid spacings of 100 and 50 km, respectively, projected onto a Lambert conformal grid (Fig. 5). The ECMWF TOGA analyses from 0000 UTC 5 November 1986 were used to initialize the model. During the ensuing 48-h simulation, grid 1 boundary conditions were updated every 12 h with the ECMWF TOGA data while the grid 2 boundary conditions were updated every 1 h with output from the grid 1 simulation.

Model physics include a cloud-sensitive radiation scheme, a mixed-phase cloud scheme, and a five-layer predictive soil model (Dudhia 1996). The boundary layer scheme developed by Hong and Pan (1996) was implemented along with the Kain and Fritsch (1993) cumulus parameterization. The model employs a terrain-following sigma (σ) coordinate system with 23 half- σ levels in the vertical. Output from the model simulation was interpolated to 20 isobaric levels at 50-hPa intervals from 1000 to 50 hPa.

Although systematic evaluation of the model simulation will not be presented here, a limited verification of its output is offered. Shown in Fig. 6 are the positions of the SLP minima from the ECMWF analyses and MM5 forecasts, along with their respective intensities, at 12-h intervals from 0000 UTC 5 November to 0000 UTC 7 November. Though the model simulation understates the rapid development of the cyclone from 0000 to 1200 UTC 5 November, it still describes a remarkable 16 hPa of deepening in 12 h. The model continues its slight deepening in the next 12 h, a period during which the analyses suggest stasis. Finally, the model understates the rapidity of the surface cyclolysis from 0000 to 1200 UTC 6 November by 3 hPa. Despite these differences, the MM5 produces a fairly faithful simulation of this unusual event and we confidently employ the gridded output from this simulation to perform our diagnosis of this case. An important component of that diagnosis is piecewise PV inversion, which is undertaken in order to determine the relative contributions



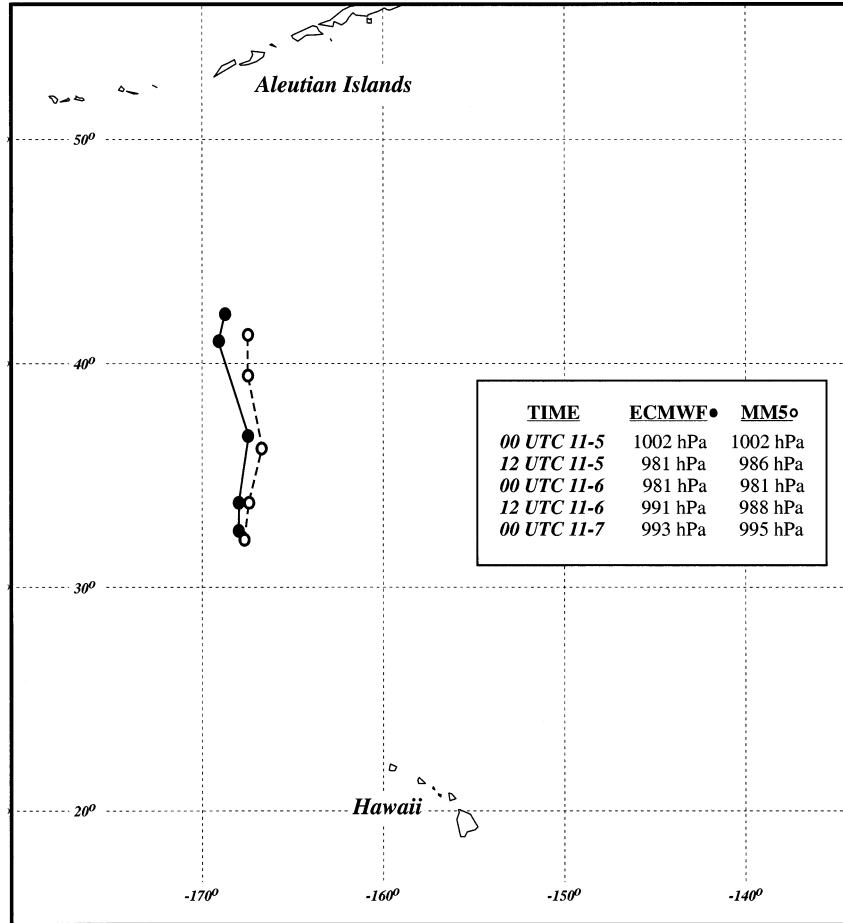


FIG. 6. Position of the SLP minimum at 12-h intervals from 0000 UTC 5 Nov to 0000 UTC 7 Nov 1986 according to the ECMWF analyses (filled black dots) and the MM5 simulation (open black circles).

of discrete pieces of the PV to the rapid fluctuations in intensity experienced by this cyclone.

4. Piecewise potential vorticity analysis

a. Technique and definitions

The Ertel potential vorticity (EPV) was first defined by Rossby (1940) and Ertel (1942) as

$$\text{EPV} = \frac{1}{\rho} \boldsymbol{\eta} \cdot \nabla \theta, \quad (1)$$

where ρ is the density, $\boldsymbol{\eta}$ is the absolute vorticity vector, and θ is the potential temperature. Two properties of the Ertel PV that make it particularly appealing as a diagnostic tool for examining aspects of the cyclone life cycle are *conservation* and *invertibility*. EPV, as defined in (1), is conserved under the full primitive equations, given adiabatic, inviscid flow. Invertibility refers to the fact that, given a balance condition relating the mass

and momentum fields and a suitable set of boundary conditions on a given domain, knowledge of the PV distribution within the domain is sufficient to recover the full kinematic and thermodynamic structure of the atmosphere within that domain. Davis and Emanuel (1991, hereafter DE) developed a functioning scheme, based upon the Charney nonlinear balance (Charney 1955), for inversion of the full Ertel PV. Their scheme assumes 1) hydrostatic balance and 2) that the magnitude of the irrotational component of the wind is much smaller than the magnitude of the nondivergent component (i.e., $|\mathbf{V}_\chi| \ll |\mathbf{V}_\psi|$). Applying these approximations to the divergence equation and (1) results in the invertibility relationship for this system (DE):

$$\nabla^2 \Phi = \nabla \cdot (f \nabla \psi) + \frac{2}{a^4 \cos^2 \phi} \frac{\partial \left(\frac{\partial \psi}{\partial \lambda}, \frac{\partial \psi}{\partial \phi} \right)}{\partial (\lambda, \phi)} \quad \text{and} \quad (2)$$

$$\text{EPV} = \frac{g\kappa\pi}{p} \left[(f + \nabla^2\psi) \frac{\partial^2\Phi}{\partial\pi^2} - \frac{1}{a^2 \cos^2\phi} \frac{\partial^2\psi}{\partial\lambda\partial\pi} \frac{\partial^2\Phi}{\partial\lambda\partial\pi} - \frac{1}{a^2} \frac{\partial^2\psi}{\partial\phi\partial\pi} \frac{\partial^2\Phi}{\partial\phi\partial\pi} \right], \quad (3)$$

where Φ is the geopotential, ψ is the nondivergent streamfunction, λ is the longitude, ϕ is the latitude, a is the radius of the earth, $\kappa = R/c_p$, p is pressure, and π is the Exner function [$c_p(p/p_o)^\kappa$], which serves as the vertical coordinate. Davis et al. (1996) demonstrated that (2), the Charney nonlinear balance equation (Charney 1955), is an excellent approximation to observed flows, thus validating the application of PV diagnostics to the real atmosphere.

Using PV computed from the model's wind and temperature fields at all vertical levels over grid 2, a total (or full) inversion is performed, solving this system of two equations simultaneously for ψ and Φ , with ψ and Φ prescribed on the lateral boundaries and their vertical derivatives specified on the top and bottom boundaries. The potential temperature at 975 and 75 hPa (linearly interpolated between 950 and 1000 hPa and 50 and 100 hPa, respectively) provide these Neumann boundary conditions on the horizontal boundaries. Following DE, negative values of PV are set to a small positive constant value (0.01 PVU, where 1 PVU = $10^{-6} \text{ m}^2 \text{ K kg}^{-1} \text{ s}^{-1}$). For a complete description of the boundary conditions, as well as the numerical methods used to solve the system of equations, the reader is referred to DE.

Davis and Emanuel (1991) also developed a method for piecewise PV inversion designed to isolate the mass and momentum fields associated with discrete perturbation PV anomalies. The particular specifications of the DE scheme implemented here include use of a time mean (to define perturbations) and employment of relative humidity (RH) criteria similar to that described in Korner and Martin (2000), Martin and Marsili (2002), and Posselt and Martin (2004). The time mean was composed of three consecutive 48-h simulations; one initialized at 0000 UTC 3 November, the object run described in section 2 (i.e., the run upon which the analyses were to be carried out), and another initialized at 0000 UTC 7 November. All three simulations were run in the manner described in section 2. Once this time mean was computed, it was subtracted from the instantaneous PV distribution at each discrete time in the object run. The difference between the instantaneous and the time mean PV is referred to as the perturbation PV for that time. The invertibility relationship for the perturbation PV, as well as the boundary conditions used in the solution, were the same as those used by DE [see their Eqs. (2.10) and (2.11)].

The piecewise PV inversion in the present study proceeded from a conventional three-way partitioning of the total perturbation PV field into an upper layer, an interior layer, and a surface layer. The upper layer ex-

tends from 700 to 50 hPa and is designed to isolate PV anomalies associated with undulations in the tropopause. Accordingly, we set the positive perturbation PV in this layer to 0.0 PVU whenever the relative humidity was greater than or equal to 70%. The interior layer extends from 850 to 150 hPa and is designed to isolate tropospheric PV anomalies associated with latent heat release. Given that latent heat release occurs in environments at or near saturation, the positive perturbation PV in this layer is set to 0.0 PVU whenever the relative humidity is less than 70%. This guards against that the scheme mistaking extruded stratospheric perturbation PV for perturbation PV "produced" by latent heat release. Finally, the surface layer, designed to isolate the boundary potential temperature anomalies that are equivalent to PV anomalies just above the surface (Bretherton 1966), includes both the 975-hPa potential temperature and all perturbation PV in the 950–900-hPa layer.

The combination of the three layers and their respective relative humidity criteria excludes only two parts of the total perturbation PV distribution from being inverted, namely, 1) positive perturbation PV in air with relative humidity greater than 70% in the 100–50-hPa layer and 2) perturbation PV in air with relative humidity less than 70% in the 850–700-hPa layer. Careful scrutiny of the data, however, revealed that these portions of the total perturbation PV distribution were very small (in magnitude or spatial scale or both) in the present case. For the remainder of the paper U_{pert} will refer to perturbations associated with the upper layer, M_{pert} to perturbations associated with the interior layer, and L_{pert} to perturbations associated with the surface layer.

b. Evaluation

Once the inversion was performed, the effect of each of the three pieces of the perturbation PV on the lower-tropospheric height changes during the cyclone's life cycle was considered. Since the lowest available isobaric surface in the inversion output was 950 hPa, subsequent analysis will concentrate on the evolution of geopotential height at that level. The location and intensity of the 950-hPa full inversion height minima are compared to the model 950-hPa height minima in Fig. 7. Notice that the geographic location of the different 950-hPa geopotential height minima compare very well. For the most part, the model heights are slightly higher than the full inversion heights though the difference is not large at any time. Another important test of the results of the piecewise inversion is to compare the sum of the partitioned heights to the full inversion heights. The sum of the three major partitions and other small residuals is never more than 5% different from the full inversion heights (not shown). Thus, we confidently employ the results of the piecewise inversion to investigate the nature of this cyclone's life cycle.

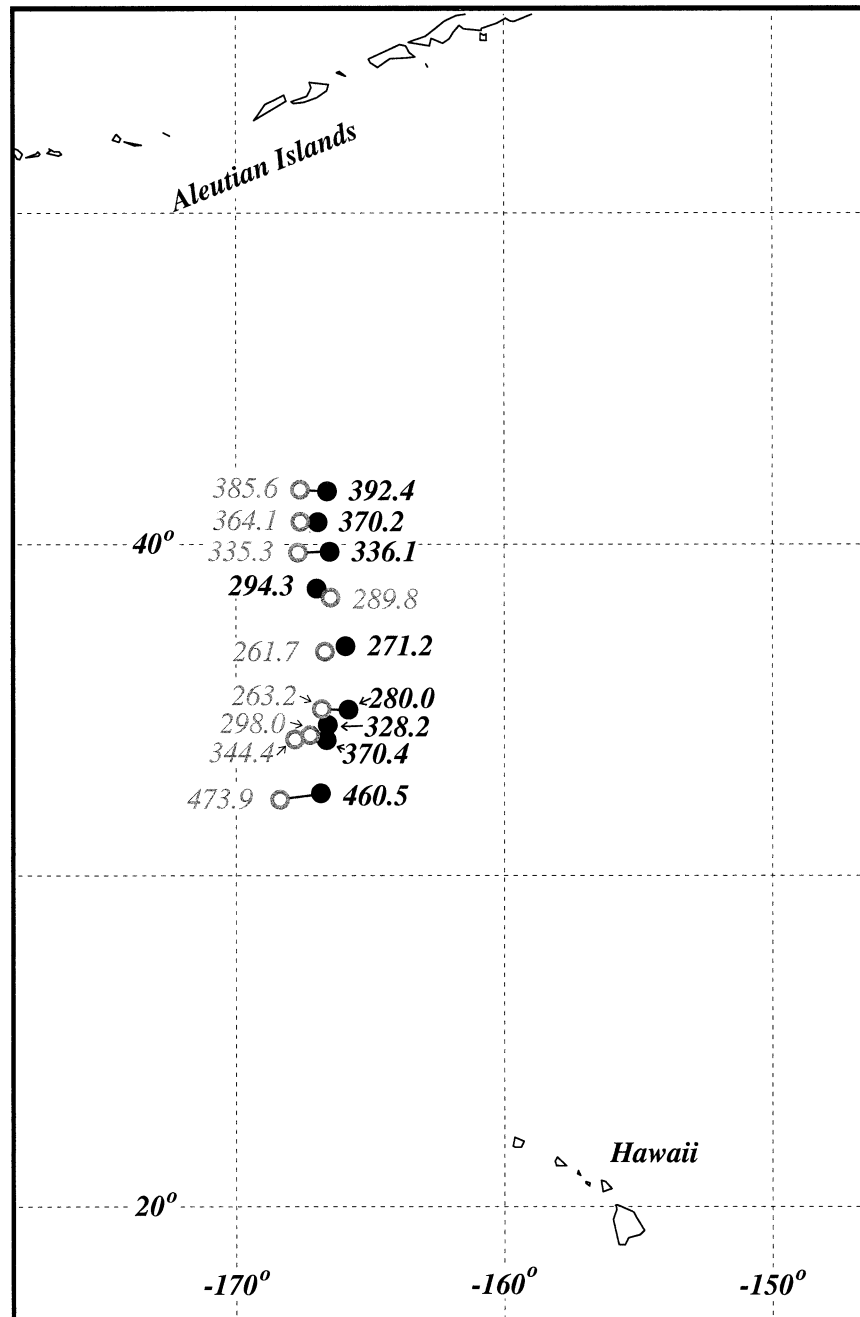


FIG. 7. Positions of the 950-hPa geopotential height minima at 6-h intervals from 0000 UTC 5 Nov to 0000 UTC 7 Nov 1986 from the MM5 output (solid black circles) and the full inversion output (open gray circles). The 950-hPa geopotential heights from the model output (bold black numbers) and the full inversion output (thin gray numbers) are given adjacent to the dots.

c. Partitioned height changes

Figure 8 shows the 950-hPa geopotential height anomalies associated with the U_{pert} PV anomaly at 12-h intervals from 0000 UTC 5 November to 1200 UTC 6 November 1986. A number of changes occur during this 36-h period. First, the negative U_{pert} height anomaly shrinks in size and magnitude throughout the period

with the most significant size and magnitude changes occurring from 0000 to 1200 UTC 6 November (Figs. 8c,d). Throughout the period the center of the negative U_{pert} height anomaly migrates southward. Second, the rapid development of a positive U_{pert} height anomaly south of the Aleutian Islands takes place between 1200 UTC 5 November and 1200 UTC 6 November (Figs.

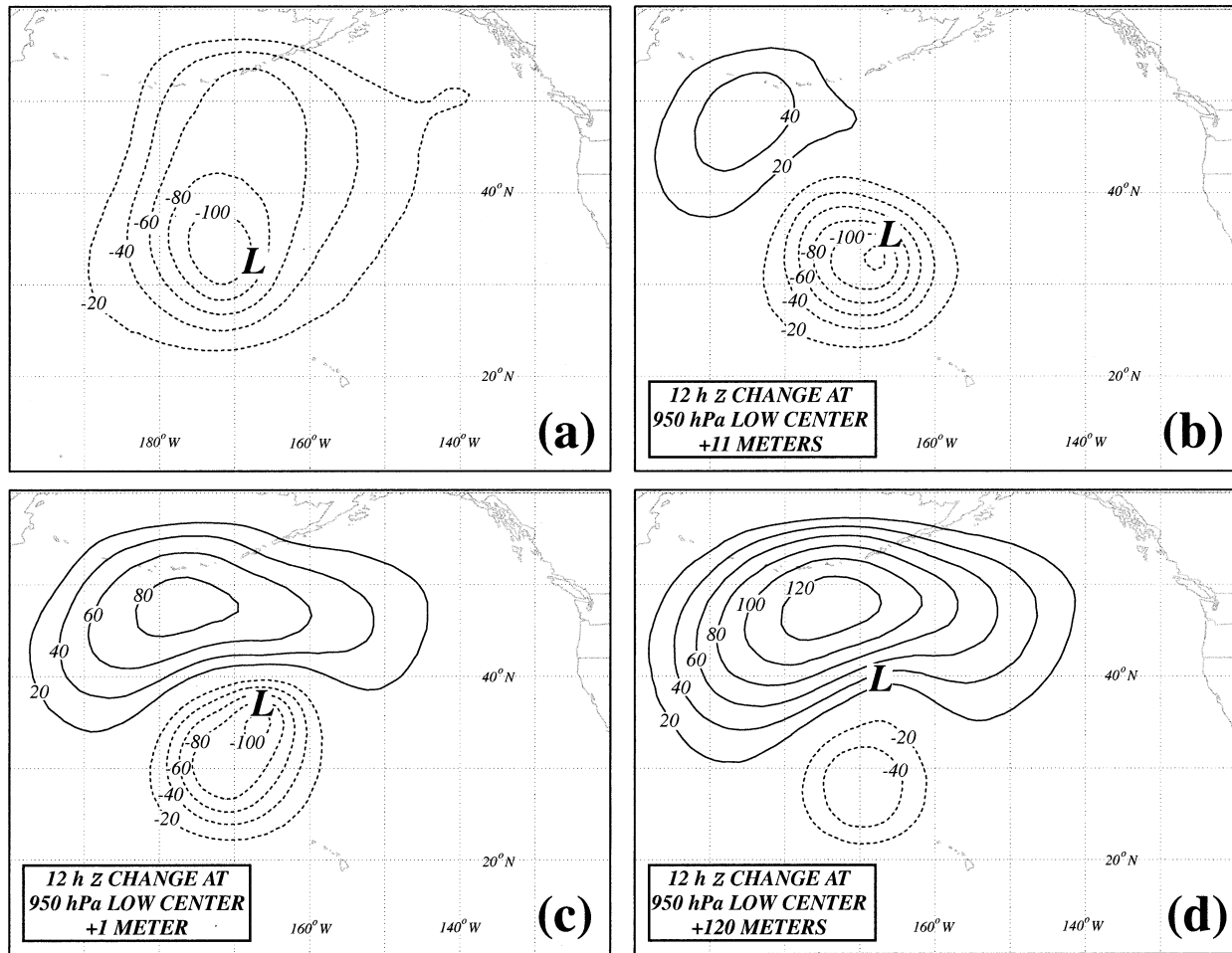


FIG. 8. (a) The 950-hPa geopotential height perturbation associated with the U_{pert} PV anomaly at 0000 UTC 5 Nov 1986. Negative (positive) geopotential height perturbations are indicated by dashed (solid) lines labeled in m and contoured every 20 m. The L indicates the position of the 950-hPa full inversion geopotential height minimum at 0000 UTC 5 Nov 1986. (b) As for (a) except for 1200 UTC 5 Nov 1986. (c) As for (a) except for 0000 UTC 6 Nov 1986. (d) As for (a) except for 1200 UTC 6 Nov 1986.

8b–d). Third, the surface cyclone center moves northward away from the center of negative U_{pert} height anomaly and toward the developing perturbation ridge throughout the period. These changes conspire to produce significant U_{pert} height changes (+120 m) at the positions of the full inversion height minimum in the 12-h period ending at 1200 UTC 6 November (Fig. 8d).

A similar analysis for the contributions to height changes associated with lower-tropospheric temperature anomalies is garnered by considering the L_{pert} height anomalies (Fig. 9). Throughout the period the height changes associated with L_{pert} are modest. A 15-m height fall is associated with an intensification of the lower-tropospheric warm anomaly during the cyclogenetic period (Fig. 9b). Despite the fact that the lower-tropospheric circulation intensifies the warm anomaly associated with the cyclone, the full inversion height minimum remains on the periphery of the warm anomaly and consequently the warm anomaly contributes only modest height falls in the subsequent 24 h (Figs. 9c,d).

The presence of strongly negative height anomalies to the north and east of the lower-tropospheric cyclone center at these later times is characteristic of deeply occluded cyclones in which the peak of the warm sector is often at a considerable distance to the north and east of the cyclone center.

The effect of latent heat release on this cyclone's life cycle can be assessed by considering the height perturbations associated with the M_{pert} PV anomaly (Fig. 10). During the explosive cyclogenesis period of the life cycle (0000–1200 UTC 5 November), 112 m of height fall at the low center are contributed by the M_{pert} PV anomaly. Little additional change to the height minimum is contributed by the subsequent latent heat release during this storm, though a robust negative height perturbation is maintained through 1200 UTC 6 November (Fig. 10d).

Finally, Fig. 11 offers a summary of the 6-hourly evolution of height changes at the 950-hPa geopotential height minimum. The full inversion height changes

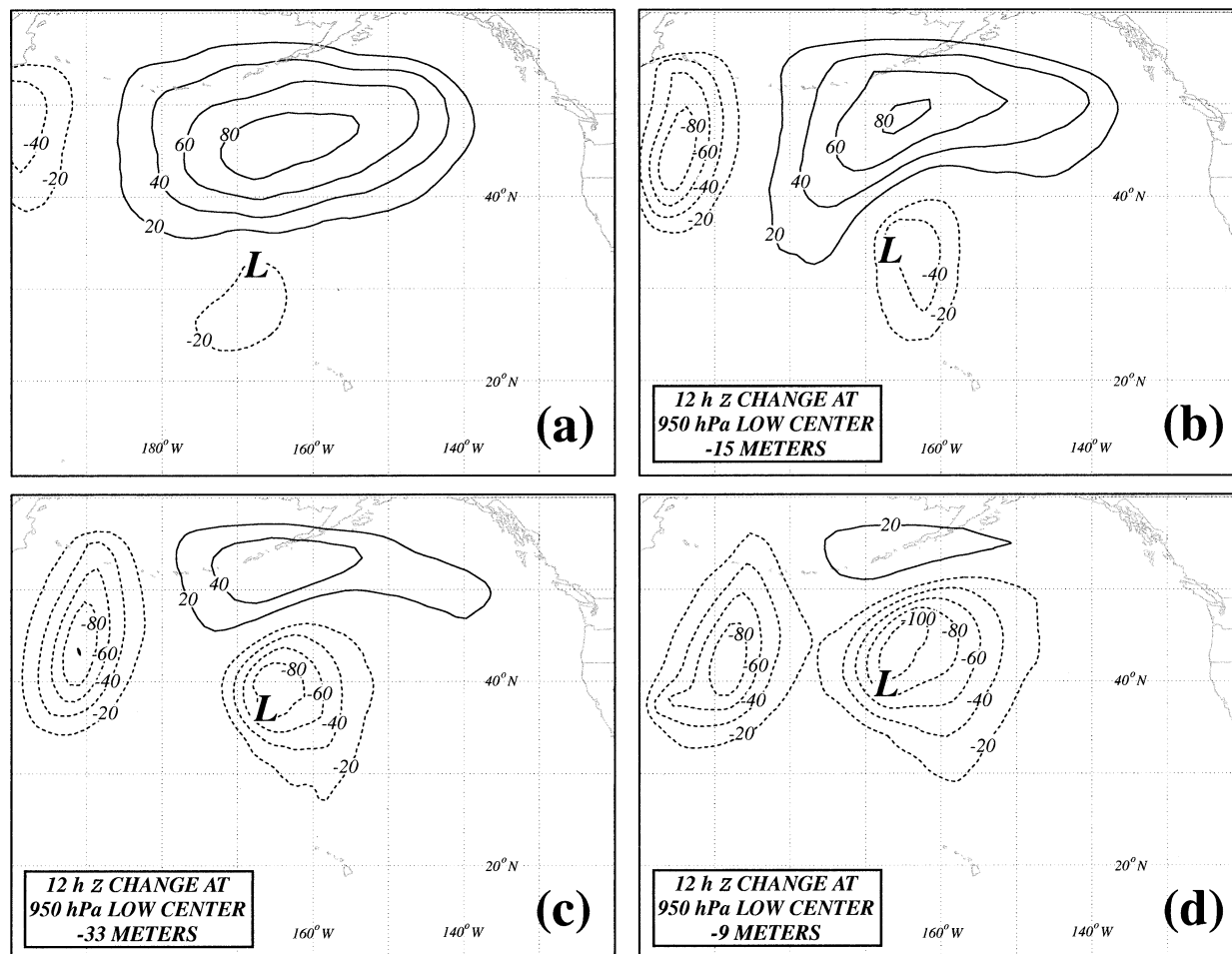


FIG. 9. As for Fig. 8 except for 950-hPa geopotential height perturbations associated with the L_{pert} PV anomaly at (a) 0000 UTC 5 Nov, (b) 1200 UTC 5 Nov, (c) 0000 UTC 6 Nov, and (d) 1200 UTC 6 Nov 1986.

compare well with the model height changes (Fig. 11a).⁴ Partitioning of the full inversion perturbation height changes into the contributions from the three pieces of the perturbation PV demonstrates that the M_{pert} piece contributes the most to the rapid cyclogenesis phase while the U_{pert} piece contributes the most to the abrupt cyclolysis phase (Fig. 11b). The L_{pert} piece contributes modestly but steadily to development throughout most of the life cycle.

The preceding analysis suggests that a pulse of latent heat release early in the development of this storm contributed to the explosive growth of the surface cyclone. Rapid growth of a U_{pert} perturbation ridge in the lower troposphere provided the greatest contribution to the subsequent abrupt cyclolysis. Using output from the MM5, the nature of this pulse of latent heat release and its relationship to the growth of the high-latitude perturbation ridge is explored in the next section.

⁴ Model height changes were evaluated by subtracting the heights at the cyclone center at time T from heights at the cyclone center at time $T + 6$ h.

5. Latent heat release and the growth of the U_{pert} PV ridge

a. Latent heat release

The latent heat release that characterized the development phase of the primary cyclone was associated with a burst of convection. A number of prior studies have shown that heavy rain events in the subtropical central Pacific are often characterized by weak instability in the lower troposphere (e.g., Schroeder 1977, 1981; Kodama and Barnes 1997). In their investigation of heavy rain events on the southeast slopes of the Mauna Loa volcano on the island of Hawaii, Kodama and Barnes (1997) found that the K index (KI) was the only useful predictor for heavy rain from among several standard stability indices. The KI, given by

$$\text{KI} = T_{850} - T_{500} + T_{d850} - T_{dd700} \quad (4)$$

(where T_{dd} is the dewpoint depression), measures middle-tropospheric stability as well as the availability of moisture in the lower and middle troposphere (George

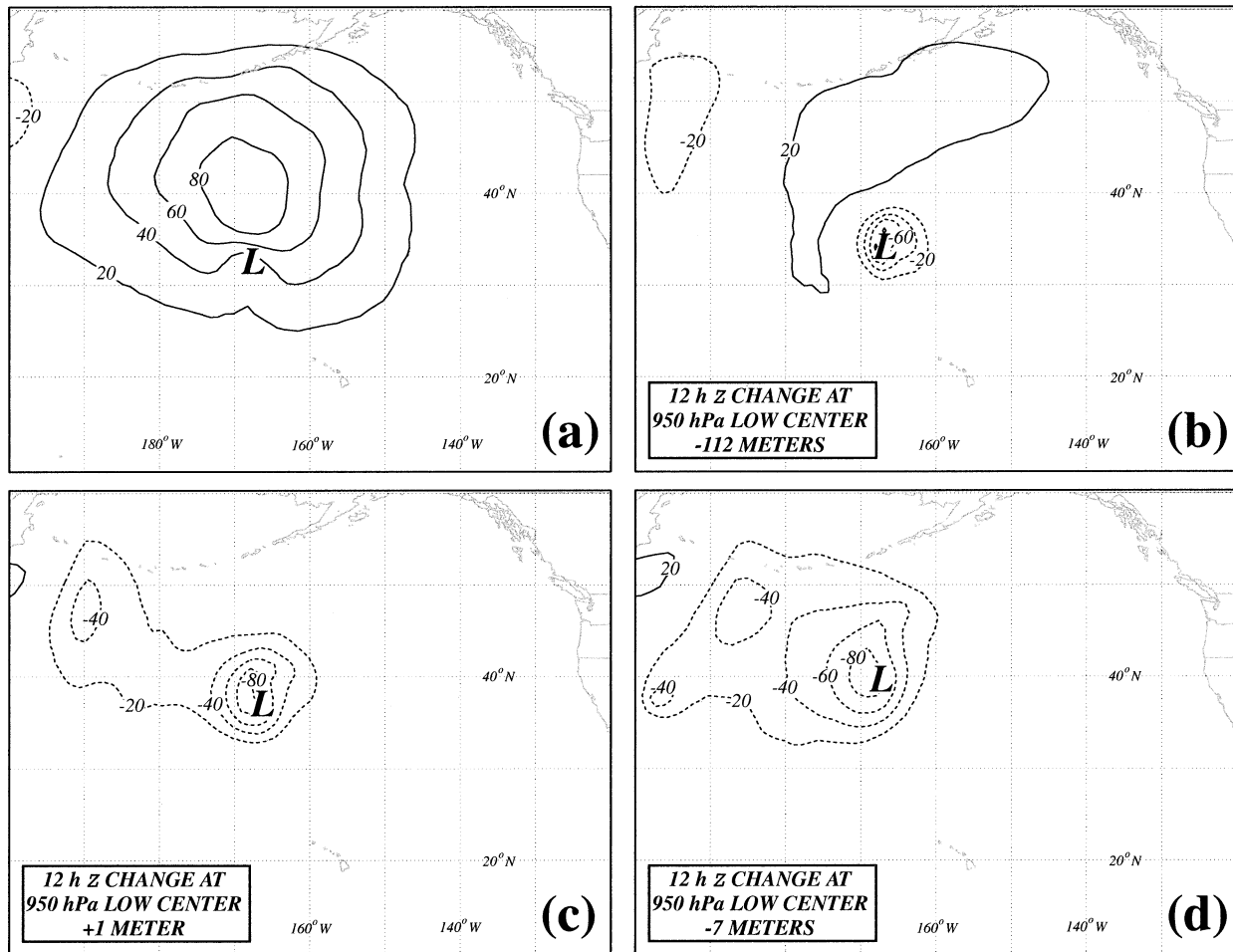


FIG. 10. As for Fig. 8 except for 950-hPa geopotential height perturbations associated with the M_{pert} PV anomaly at (a) 0000 UTC 5 Nov, (b) 1200 UTC 5 Nov, (c) 0000 UTC 6 Nov, and (d) 1200 UTC 6 Nov 1986.

1960). Kodama and Barnes (1997) found that the average KI of the heavy rain events they studied was 33.

The heavy precipitation that characterized the development phase of the primary cyclone was produced by frontogenetical forcing⁵ for ascent in an environment of high KI. Evidence for the presence of these ingredients, and their consequences, is displayed in Fig. 12. The MM5 reflectivity at 0300 UTC 5 November indicates a region of greater than 35 dBZ to the east of the surface cyclone center (Fig. 12a). The model convection occurred in a region of KI greater than 30 (Fig. 12c) superimposed with 850-hPa frontogenetic forcing for ascent (Fig. 12e).

Six hours later, equally intense convective activity (Fig. 12b) again was associated with the juxtaposition of the high KI values (Fig. 12d) with intense 850-hPa positive frontogenesis (Fig. 12f). Similar circumstances prevailed until about 1500 UTC 5 November (not

shown) when the convection subsided in intensity. An interesting consequence of this burst of convective heating was the development of a PV tower extending from the surface into the upper troposphere by 0600 UTC 5 November (Fig. 13). This feature bears a striking resemblance to the characteristic PV tower observed in association with tropical cyclones (Shapiro and Franklin 1995; Smallcomb 1999).

b. Growth of the U_{pert} PV ridge

The rapid height rises that occurred during the cyclolysis phase of this storm's life cycle were a direct result of the migration of the cyclone northward into a strengthening perturbation ridge associated with the tropopause PV anomaly. The growth of this perturbation ridge and its relationship to the tropopause perturbation PV is shown in Fig. 14. At 0000 UTC 5 November a significant negative perturbation PV feature was located at the western end of the Aleutians while a more modest negative PV feature was located near the deepening sur-

⁵ We used the 2D Petterssen (1936) frontogenesis function employing the full wind and θ distributions at 850 hPa.

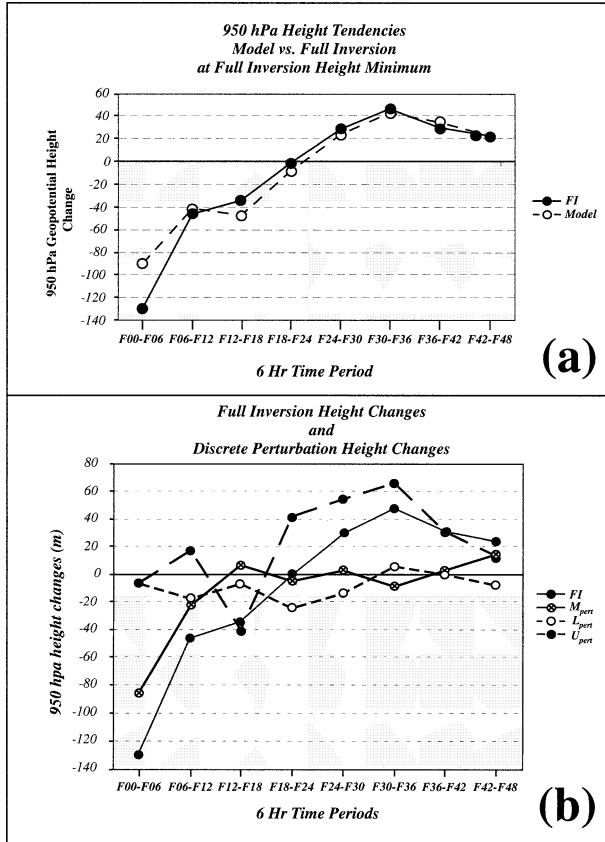


FIG. 11. (a) The 6-h height changes at the position of the 950-hPa geopotential height minimum from the full MM5 simulation (open circles) and the sum of the partitioned heights (solid circles). (b) The 6-h height changes at the position of the 950-hPa geopotential height minimum from the sum of the partitioned perturbation heights (gray circles) and the three discrete perturbation heights (open circle, L_{pert} ; solid circle, U_{pert} ; and cross-filled circle, M_{pert}).

face cyclone itself (Fig. 14a). We shall refer to these two perturbation PV features as the western and eastern PV features, respectively. By 1200 UTC 5 November, the western PV feature had moved southeastward while the eastern PV feature had become more negative and of larger horizontal scale (Fig. 14b). The two negative PV features were much closer to one another at this time. Also, a perturbation geopotential ridge associated with the western PV feature was just beginning to develop south of the Aleutians.

Twelve hours later the continued southeastward movement of the western PV feature, coupled with the continued blossoming of the eastern PV feature, had led to a nearly continuous swath of negative perturbation PV across the North Pacific basin south of the Aleutian Islands (Fig. 14c). Associated with this more widespread and continuous region of negative perturbation PV was a perturbation geopotential ridge that occupied the same region (Fig. 14c). The surface cyclone, continuing its northward path, was headed directly into the burgeoning ridge. By 1200 UTC 6 November, the perturbation PV

ridge had further strengthened as the western PV feature (directly associated with the positively tilted upper ridge located upstream of the primary cyclone; see Figs. 1b–4b) continued its southeastward movement while the eastern PV feature migrated north and northeastward (Fig. 14d). Note that by this time the surface cyclone had moved northward into the positive perturbation height region. Thus, the growth of the 950-hPa geopotential ridge was the result of two factors: 1) the persistent southeastward movement of the western PV feature and 2) the growth and subsequent northward and northeastward migration of a significant negative perturbation PV feature to the northeast of the surface cyclone. These two tendencies led to the juxtaposition of the two features by ~0000 UTC 6 November and the subsequent rapid rise in perturbation geopotential height south of the Aleutians.

The growth of the eastern PV feature was directly related to the latent heat released during the convective burst that characterized the rapid cyclogenesis phase of this cyclone's life cycle. Insight into this development arises from consideration of the PV tendency equation:

$$\frac{\partial PV}{\partial t} = -\mathbf{V} \cdot \nabla PV + \frac{dPV}{dt}, \quad (5)$$

where $\nabla = (\partial/\partial x)\hat{i} + (\partial/\partial y)\hat{j} + (\partial/\partial z)\hat{k}$. The full PV field is composed of a time mean (\overline{PV}) and a perturbation (PV') so that (5) can be recast as

$$\frac{\partial(PV')}{\partial t} = -\mathbf{V} \cdot \nabla(PV) + \frac{d(PV)}{dt} \quad (6)$$

since the local time tendency of the mean PV is zero by definition. Thus, the local change in the perturbation PV is forced by the sum of the Lagrangian changes and PV advection. Lagrangian changes in PV can arise from turbulent diffusion and mixing, friction, or diabatic processes. Given the previously established major role of latent heat release in the cyclogenesis phase of this storm, our analysis of the Lagrangian rate of change of PV will concentrate on the effects of latent heat release (LHR).

Calculation of LHR was made directly from the model output following a method introduced by Emanuel et al. (1987) and employed by Cammas et al. (1994) as

$$H = \omega \left(\frac{\partial \theta}{\partial p} - \frac{\gamma_m}{\gamma_d} \frac{\theta}{\theta_e} \frac{\partial \theta_e}{\partial p} \right), \quad (7)$$

where H corresponds to LHR, ω is the vertical motion (in hPa s⁻¹), θ_e is the equivalent potential temperature, and γ_d and γ_m are the dry- and moist-adiabatic lapse rates, respectively. Using this value of latent heating, quantitative calculations of the diabatic time tendency of PV were made. Again, following Cammas et al. (1994), the expression can be written as

$$\frac{d(PV)}{dt} = -g \nabla_p \cdot \mathbf{Y}, \quad (8)$$

0300 UTC 5 November 1986 0900 UTC 5 November 1986

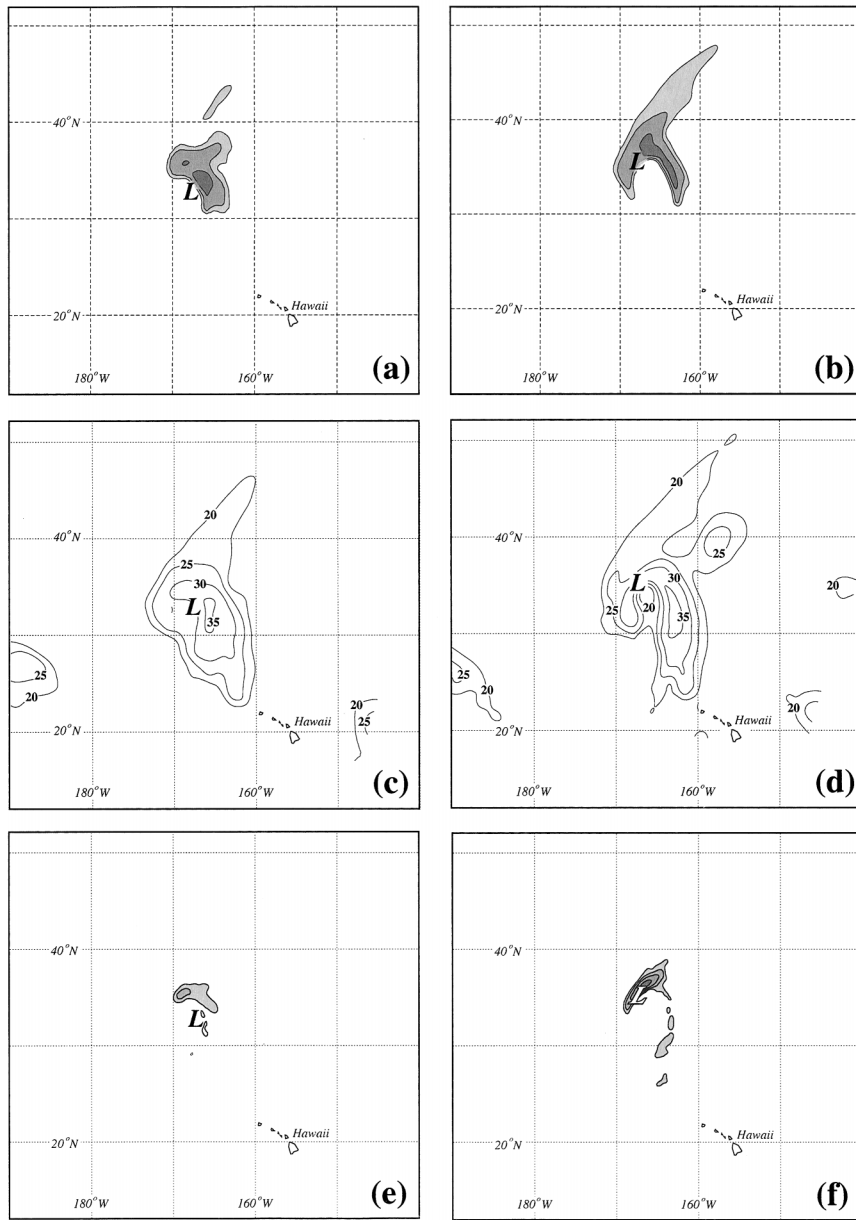


FIG. 12. (a) The 3-h forecast of MM5 radar reflectivity valid at 0300 UTC 5 Nov 1986. Reflectivity contoured in dBZ and shaded every 5 dBZ beginning at 25 dBZ. Bold **L** indicates the position of the surface low pressure center. (b) As for (a) but for 9-h forecast valid at 0900 UTC 5 Nov 1986. (c) The 3-h forecast of MM5 KI valid at 0300 UTC 5 Nov 1986. The KI is contoured every 5 beginning at 20. Bold **L** as for (a). (d) As for (c) but for 9-h forecast valid at 0900 UTC 5 Nov 1986. (e) The 3-h forecast of 850-hPa frontogenesis valid at 0300 UTC 5 Nov 1986. Frontogenesis labeled in units of $K (100 \text{ km})^{-1} \text{ day}^{-1}$ and shaded every 2 and 4 $K (100 \text{ km})^{-1} \text{ day}^{-1}$. Bold **L** as for (a). (f) As for (e) but for 9-h forecast valid at 0900 UTC 5 Nov 1986. Frontogenesis contoured and shaded every 2, 5, 10, and 20 $K (100 \text{ km})^{-1} \text{ day}^{-1}$.

where g is the gravitational acceleration and ∇_p is the 3D gradient operator ($\nabla_p = (\partial/\partial x)\hat{i} + (\partial/\partial y)\hat{j} - (\partial/\partial p)\hat{k}$). Here, \mathbf{Y} is the *nonadvective* PV flux vector:

$$\mathbf{Y} = -H\zeta_a + \nabla_p \theta \times \mathbf{F}, \quad (9)$$

where ζ_a is the 3D absolute vorticity vector ($\zeta_x = \partial v/\partial p$, $\zeta_y = -\partial u/\partial p$, $\zeta_p = f$) and \mathbf{F} is the friction vector. For our purposes, neglecting friction, an expression for the PV tendency associated with LHR can be written as

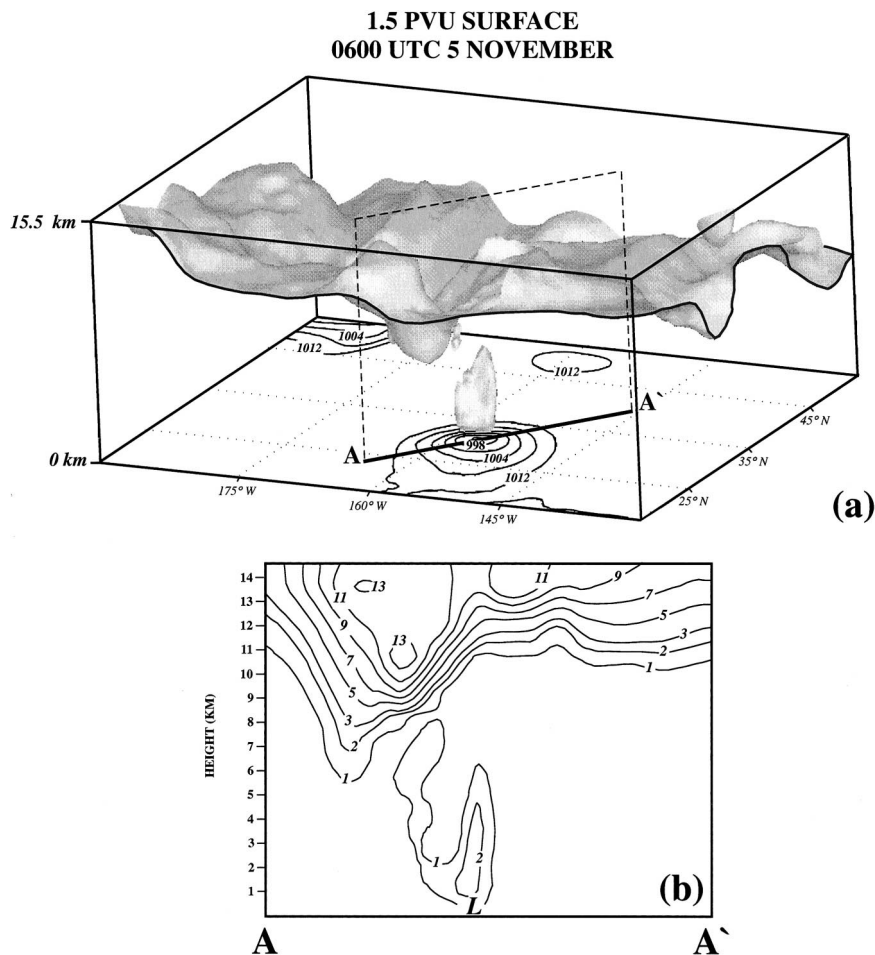


FIG. 13. (a) The 1.5-PVU surface and SLP from the 6-h forecast of the MM5 valid at 0600 UTC 5 Nov 1986. The 1.5-PVU surface is shaded with the border outlined on the facing sides of the 3D box. SLP is labeled in hPa and contoured every 4 hPa ending at 1012 hPa. Note the PV tower directly atop the SLP minimum as is often the case for tropical cyclones. Cross section along line A–A' is shown in (b). (b) Vertical cross section of potential vorticity along line A–A' in (a). The PV is labeled and contoured in PVU in intervals of 1, 2, 3, 5, 7, 9, 11, and 13 PVU. Bold *L* denotes position of SLP minimum.

$$\frac{d(\text{PV})}{dt} = -g \nabla_p \cdot \mathbf{Y} = g \zeta_a \cdot \nabla_p H. \quad (10)$$

According to this relationship, the concentration and/or dilution of PV depends directly on the gradient of the diabatic heating in the direction of the absolute vorticity vector. Where the vertical component of the vorticity dominates, vertical redistribution of PV occurs, resulting in reduced PV above the region of LHR and increased PV below. Using (10), we can rewrite (6) as

$$\frac{\partial(\text{PV}')}{\partial t} = -V \cdot \nabla(\text{PV}) + g \zeta_a \cdot \nabla_p H, \quad (11)$$

which demonstrates that local changes in the perturbation PV are forced by the combination of PV advection and PV redistribution via latent heat release.

Figure 15 shows the contributions to the negative PV tendency made by diabatic and advective processes in

the region surrounding the eastern PV feature at 6-h intervals from 0000 to 1800 UTC 5 November. At 0000 UTC 5 November the region of negative tropopause perturbation PV is overwhelmingly associated with a negative diabatic PV tendency (Fig. 15a). The largest values of this tendency ($-0.1 \text{ PVU } 6 \text{ h}^{-1}$) are directly related to the intense convective heating characterizing the primary cyclone at this time. Lesser values of PV tendency to the north and northeast of the cyclone are associated with instantaneous PV advection (Fig. 15e). Clearly, the combined effects of LHR and PV advection were acting to intensify and expand the eastern PV feature at this time.

Expansion of this feature continued to be fueled by the combination of LHR and PV advection through 0600 UTC 5 November (Figs. 15b,f). As before, the largest values of the negative PV tendency ($-0.05 \text{ PVU } 6 \text{ h}^{-1}$) were a direct result of the intense LHR near the cyclone

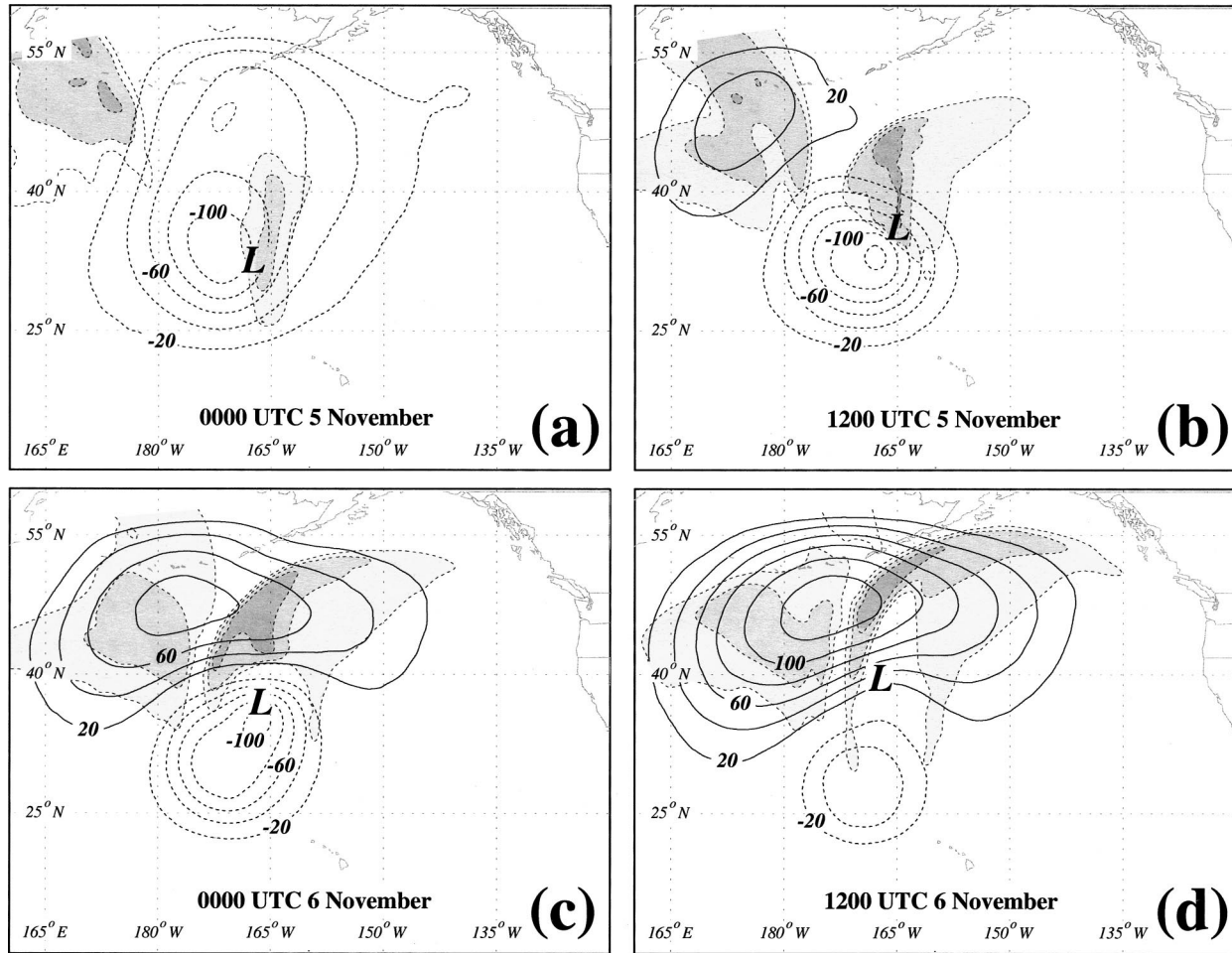


FIG. 14. (a) The 950-hPa U_{pert} geopotential height anomaly (thick dashed line) and 250–300-hPa negative perturbation PV anomaly (shaded) from the MM5 simulation at 0000 UTC 5 Nov 1986. The U_{pert} heights are labeled in m and contoured every 20 m (except the zero height line). Negative perturbation PV is shaded every 1 PVU beginning at 1 PVU. (b) As for (a) but for the 12-h forecast of MM5 valid at 1200 UTC 5 Nov. Thick solid lines are for the positive 950-hPa U_{pert} geopotential height anomaly labeled and contoured as in (a). (c) As for (b) but for 24-h forecast of MM5 valid at 0000 UTC 6 Nov 1986. (d) As for (b) but for 36-h forecast of MM5 valid at 1200 UTC 6 Nov 1986.

center (Fig. 15b). The negative PV tendency seen on the northwestern edge of the negative PV feature at this time was associated with PV advection, as was the northeastward extension of the -1 PVU contour (Fig. 15f).

Growth of the negative PV feature to the north and northwest continued through 1200 UTC 5 November at which time the large negative diabatic PV tendencies near the cyclone center had diminished slightly in magnitude (Fig. 15c). The expansion to the north and northwest of the region of negative perturbation PV was a result of persistent negative PV advection in those directions (Fig. 15g). As was the case at other times, the negative PV feature at this time was located in a region of generally negative PV tendency.

Finally, by 1800 UTC 5 November, the intense PV tendencies induced by LHR (maximum value -0.1 PVU 6 h^{-1}) no longer occupied the instantaneous negative PV region but were instead to the northwest of the SLP

minimum (Fig. 15d). In fact, only modest regions of negative PV tendency occupied the negative PV region. Nonetheless, continued migration of this feature to the north and northwest was forced by PV advection (Fig. 15h). Also noteworthy is the encroachment of the western PV feature and its associated negative PV advection. After this time, the shape of the eastern PV feature changed little, though it did continue to expand to the north and northwest. The 6-h interval from 1800 UTC 5 November to 0000 UTC 6 November also coincides with the period of most rapid growth of the 950-hPa perturbation geopotential ridge that developed in response to the near merger of the western and eastern PV features. Thus, we conclude that the growth of the eastern PV feature was fueled by the same LHR that powered the explosive cyclogenesis and that its expansion to the north and northeast was propelled by negative PV advection near the tropopause. In combination with the encroachment of the western PV feature, the growth

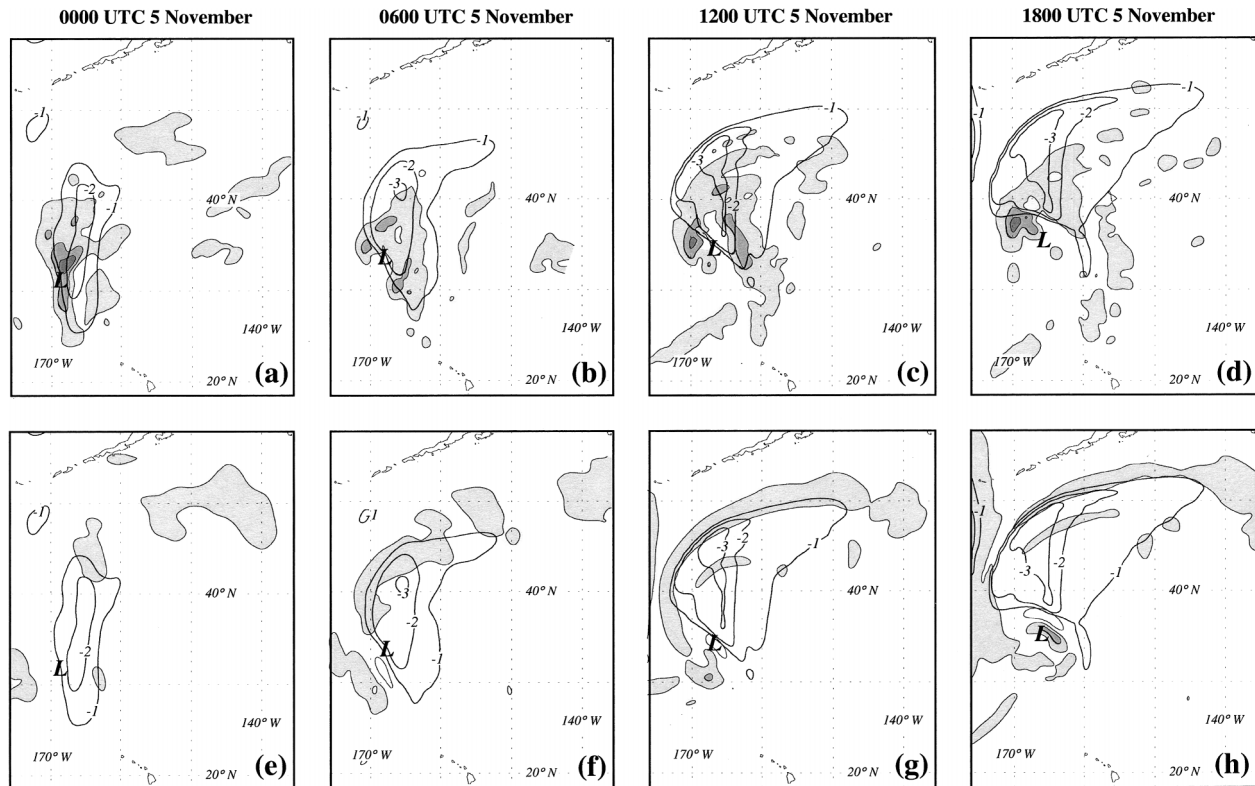


FIG. 15. (a) Diabatic PV tendency and negative perturbation PV in the 250–300-hPa layer at 0000 UTC 5 Nov 1986. Negative diabatic PV tendency labeled in 10^{-2} PVU 6 h^{-1} and shaded and contoured at -0.5 , -5.0 , and -10×10^{-2} PVU 6 h^{-1} . Negative perturbation PV labeled in PVU and contoured every -1 PVU beginning at -1 PVU. The **L** represents the location of the surface low pressure center at 0000 UTC 5 Nov 1986. (b) As for (a) except for 0600 UTC 5 Nov 1986. (c) As for (a) except for 1200 UTC 5 Nov 1986. (d) As for (a) except for 1800 UTC 5 Nov 1986. (e) Advective PV tendency and negative perturbation PV in the 250–300-hPa layer at 0000 UTC 5 Nov 1986. Negative (positive) advective PV tendency labeled in 10^{-2} PVU 6 h^{-1} and shaded and contoured at -0.5 , -5.0 (5.0), and -10 (10) $\times 10^{-2}$ PVU 6 h^{-1} with negative values shaded. Negative perturbation PV labeled in PVU and contoured every -1 PVU. The **L** represents the location of the surface low pressure center at 0000 UTC 5 November 1986. (f) As for (e) except for 0600 UTC 5 Nov 1986. (g) As for (e) except for 1200 UTC 5 Nov 1986. (h) As for (e) except for 1800 UTC 5 Nov 1986.

of the eastern PV feature contributed directly to the abrupt decay phase of this cyclone's life cycle.

6. Discussion and conclusions

In the present study a piecewise inversion of the full Ertel PV, calculated using output from a successful numerical simulation performed using the PSU–NCAR MM5, has been employed to gain insight into the life cycle of an unusual cyclone in the central Pacific Ocean. The cyclone underwent a period of explosive cyclogenesis that was followed, within 24 h, by a period of unusually rapid decay. The analysis revealed that the period of rapid cyclogenesis was almost entirely a consequence of lower-tropospheric height falls associated with a diabatically produced PV anomaly (the \mathbf{M}_{pert} PV anomaly) generated through latent heat release. The burst of convection that characterized the first 12 h of the simulation, and produced the \mathbf{M}_{pert} PV anomaly, resulted from the intrusion of a potent upper-level short wave of extratropical origin into a region of the sub-

tropical Pacific that was characterized by a weakly stratified lower troposphere.

During the explosive development stage, a positively tilted, upstream anticyclone and its associated negative tropopause-level PV anomaly (deemed the western PV feature) began a southeastward progression toward the date line, south of the Aleutian Islands. The encroachment of this western PV feature, combined with the blossoming of a negative tropopause-level PV feature associated with the developing cyclone (deemed the eastern PV feature), led to the formation of an extensive negative upper-tropospheric PV anomaly that spanned the North Pacific basin south of the Aleutian Islands by 0000 UTC 6 November. This PV anomaly was associated with a perturbation geopotential ridge at 950 hPa that continued to strengthen through 1200 UTC 6 November. The primary surface cyclone quickly progressed northward into the perturbation ridge and experienced rapid height rises as a consequence. Thus, the latent heat release that fueled the rapid development phase of the life cycle also produced a negative tro-

popause-level PV feature that, in combination with the wave encroaching from the west, produced the circumstances that eventually led to the rapid decay phase of this cyclone's life cycle.

The rapid fluctuation in intensity exhibited by this cyclone was among its most outstanding characteristics. In a paper that extended the results of the pioneering study of rapid cyclogenesis by Sanders and Gyakum (1980), Roebber (1984) found that rapidly deepening storms are characterized by longer periods of development than less intense, "ordinary" cyclones. Sutcliffe and Forsdyke (1950) introduced the notion of self-development to describe the synergistic interaction among the various physical and dynamical processes operating during cyclogenesis, which often leads to a more sustained and more robust period of development. They suggested that the lower-tropospheric warm air advection characteristically found just east of the developing surface cyclone forces geopotential height rises downstream of the upper-level short-wave trough associated with the surface cyclone. This ridge building, in turn, acts to decrease the wavelength between the trough axis and the ridge crest thereby serving to intensify the cyclonic vorticity advection (CVA) over the surface cyclone. Increased CVA promotes continued surface development, enhancing the lower-tropospheric circulation about the cyclone and reinforcing the thermal advection pattern necessary to amplify the upper-tropospheric wave structure.

The role of diabatic processes, particularly latent heat release in the comma cloud head, furthers the self-development tendency by heating the middle troposphere downstream of the upper trough axis (e.g., Uccellini 1990; Martin et al. 1993). Martin et al. (1993) described the role of latent heat release in the self-development process in terms of tropopause-level PV evolution, emphasizing the diabatic "destruction" of upper-tropospheric PV above the cloud head as a means of steepening the dynamic tropopause and intensifying surface development.

The present case clearly stands in stark contrast to the typical rapid cyclogenesis event in that the period of development lasted only 24 h. Additionally, though a potent element of the traditional self-development scenario was operating in this case (namely, latent heat release to the north and northeast of the surface cyclone center), that element conspired to inhibit, rather than assist, continued cyclonic development. Though they suggested that self-development is the preferred mode of physical and dynamical interaction during cyclogenesis, Sutcliffe and Forsdyke (1950) conceded that "self-destroying" synoptic configurations might also exist in nature. The unusual life cycle behavior of the present case might arguably be the result of such a self-destroying synoptic setting. Since the growth of a tropopause-level negative PV anomaly to the north and northeast of a cyclone is generally a direct diabatic consequence of the development itself (e.g., Martin et al. 1993), the

manner and degree to which self-development will occur in a given cyclogenesis event may well be determined by the nature of the upstream flow. In the present case, that upstream flow was characterized by a positively tilted, upper-tropospheric ridge that was associated with a negative PV anomaly near the tropopause (the western PV feature). The steady progress of that feature toward the cyclone environment led to the establishment of an extensive perturbation ridge in the lower troposphere just north of the cyclogenetic region. The northward movement of the surface cyclone into this ridge forced the abrupt cyclolysis that characterized the late stages of the life cycle of this storm. It thus appears that *self-development*, though a powerful conceptualization, underemphasizes the role played by larger-than-cyclone scales in orchestrating the manner and intensity of the dynamical and physical interactions that characterize the process of cyclogenesis. We suggest a more accurate view arises by considering the larger scales as organizing and facilitating the interactive elements that together constitute a self-developmental scenario.

Acknowledgments. The authors thank the European Centre for Medium Range Weather Forecasts (ECMWF) for supplying the ECMWF TOGA dataset used in this study. The comments of three anonymous reviewers greatly enhanced the presentation of this research. This work was sponsored by the National Science Foundation under Grants ATM-9733127 and ATM-0202012.

REFERENCES

- Anthes, R. A., Y.-H. Kuo, and J. R. Gyakum, 1983: Numerical simulations of a case of explosive cyclogenesis. *Mon. Wea. Rev.*, **111**, 1174–1188.
- Bosart, L. F., C.-C. Lai, and E. Rogers, 1995: Incipient explosive marine cyclogenesis: Coastal development. *Tellus*, **47**, 1–29.
- Bretherton, F. P., 1966: Baroclinic instability and the shortwave cutoff in terms of potential vorticity. *Quart. J. Roy. Meteor. Soc.*, **92**, 335–345.
- Cammas, J.-P., D. Keyser, G. Lackmann, and J. Molinari, 1994: Diabatic redistribution of potential vorticity accompanying the development of an outflow jet within a strong extratropical cyclone. Preprints, *Int. Symp. on the Life Cycles of Extratropical Cyclones*, Bergen, Norway, Amer. Meteor. Soc., 403–409.
- Charney, J., 1955: The use of the primitive and balance equations. *Tellus*, **7**, 22–26.
- Colucci, S. J., and T. L. Alberta, 1996: Planetary-scale climatology of explosive cyclogenesis and blocking. *Mon. Wea. Rev.*, **124**, 2509–2520.
- Davis, C. A., and K. A. Emanuel, 1991: Potential vorticity diagnostics of cyclogenesis. *Mon. Wea. Rev.*, **119**, 1929–1953.
- , E. D. Grell, and M. A. Shapiro, 1996: The balanced dynamical nature of a rapidly intensifying oceanic cyclone. *Mon. Wea. Rev.*, **124**, 3–26.
- Dudhia, J., 1996: A multi-layer soil temperature model for the MM5. Preprints, *Sixth PSU/NCAR Mesoscale Model User's Workshop*, Boulder, CO, NCAR, 49–50.
- Emanuel, K. A., M. Fantini, and A. J. Thorpe, 1987: Baroclinic instability in an environment of small stability to slantwise moist convection. Part I: Two-dimensional models. *J. Atmos. Sci.*, **44**, 1559–1587.

- Ertel, H., 1942: Ein Neuer hydrodynamischer Wirbelsatz. *Meteor. Z.*, **59**, 271–281.
- George, J. J., 1960: *Weather Forecasting for Aeronautics*. Academic Press, 673 pp.
- Grell, G. A., J. Dudhia, and D. R. Stauffer, 1994: A description of the fifth-generation Penn State/NCAR Mesoscale Model (MM5). NCAR Tech. Note NCAR/TN-398+STR, 117 pp.
- Hong, S.-Y., and H.-L. Pan, 1996: Nonlocal boundary layer vertical diffusion in a medium-range forecast model. *Mon. Wea. Rev.*, **124**, 2322–2339.
- Hoskins, B. J., I. Draghici, and H. C. Davies, 1978: A new look at the ω -equation. *Quart. J. Roy. Meteor. Soc.*, **104**, 31–38.
- Kain, J. S., and J. M. Fritsch, 1993: Convective parameterization for mesoscale models: The Kain–Fritsch scheme. *The Representation of Cumulus Convection in Numerical Models*, *Meteor. Monogr.*, No. 46, Amer. Meteor. Soc., 165–170.
- Kodama, K. R., and G. M. Barnes, 1997: Heavy rain events over the south-facing slopes of Hawaii: Attendant conditions. *Wea. Forecasting*, **12**, 347–367.
- Korner, S., and J. E. Martin, 2000: Piecewise frontogenesis from a potential vorticity perspective: Methodology and a case study. *Mon. Wea. Rev.*, **128**, 1266–1288.
- Kuo, Y.-H., and R. Reed, 1988: Numerical simulation of an explosively deepening cyclone in the eastern Pacific. *Mon. Wea. Rev.*, **116**, 2081–2105.
- , M. A. Shapiro, and E. G. Donall, 1991: The interaction between baroclinic and diabatic processes in a numerical simulation of a rapidly intensifying extratropical marine cyclone. *Mon. Wea. Rev.*, **119**, 368–384.
- Manobianco, J. T., 1989: Explosive east coast cyclogenesis: Numerical experimentation and model-based diagnosis. *Mon. Wea. Rev.*, **117**, 2384–2405.
- Martin, J. E., 1998: The structure and evolution of a continental winter cyclone. Part I: Frontal structure and occlusion process. *Mon. Wea. Rev.*, **126**, 303–328.
- , and N. Marsili, 2002: Surface cyclolysis in the North Pacific Ocean. Part II: Piecewise potential vorticity diagnosis of a rapid cyclolysis event. *Mon. Wea. Rev.*, **130**, 1264–1281.
- , J. D. Locatelli, and P. V. Hobbs, 1993: Organization and structure of clouds and precipitation on the mid-Atlantic coast of the United States. Part VI: The synoptic evolution of a deep tropospheric frontal circulation and attendant cyclogenesis. *Mon. Wea. Rev.*, **121**, 1299–1316.
- , R. D. Graumann, and N. Marsili, 2001: Surface cyclolysis in the North Pacific Ocean. Part I: A synoptic climatology. *Mon. Wea. Rev.*, **129**, 748–765.
- McLay, J. G., and J. E. Martin, 2002: Surface cyclolysis in the North Pacific Ocean. Part III: Composite local energetics of tropospheric-deep cyclone decay associated with rapid surface cyclolysis. *Mon. Wea. Rev.*, **130**, 2507–2529.
- Petterssen, S., 1936: Contribution to the theory of frontogenesis. *Geophys. Publ.*, **11**, 1–27.
- Posselt, D. J., and J. E. Martin, 2004: The effect of latent heat release on the evolution of a warm occluded thermal structure. *Mon. Wea. Rev.*, **132**, 578–599.
- Reed, R. J., and M. D. Albright, 1986: Case study of explosive cyclogenesis in the eastern Pacific. *Mon. Wea. Rev.*, **114**, 2297–2319.
- Roebber, P. J., 1984: Statistical analysis and updated climatology of explosive cyclones. *Mon. Wea. Rev.*, **112**, 1577–1589.
- Rosby, C. G., 1940: Planetary flow patterns in the atmosphere. *Quart. J. Roy. Meteor. Soc.*, **66**, 68–87.
- Sanders, F., 1986: Explosive cyclogenesis in the west-central North Atlantic Ocean, 1981–1984. Part I: Composite structure and mean behavior. *Mon. Wea. Rev.*, **114**, 1781–1794.
- , and J. R. Gyakum, 1980: Synoptic-dynamic climatology of the “bomb.” *Mon. Wea. Rev.*, **108**, 1589–1606.
- Schroeder, T. A., 1977: Meteorological analysis of the Oahu flood. *Mon. Wea. Rev.*, **105**, 458–468.
- , 1981: Characteristics of local winds in northwest Hawaii. *J. Appl. Meteor.*, **20**, 874–881.
- Shapiro, L. J., and J. L. Franklin, 1995: Potential vorticity in Hurricane Gloria. *Mon. Wea. Rev.*, **123**, 1465–1475.
- Sinclair, M. R., 1997: Objective identification of cyclones and their circulation intensity and climatology. *Wea. Forecasting*, **12**, 595–612.
- , and M. J. Revell, 2000: Classification and composite diagnosis of extratropical cyclogenesis in the southwest Pacific. *Mon. Wea. Rev.*, **128**, 1089–1105.
- Smallcomb, C. C., 1999: The overland re-intensification of Tropical Storm Danny in July of 1997. M.S. thesis, Dept. of Atmospheric and Oceanic Sciences, University of Wisconsin—Madison, 170 pp. [Available from Dept. of Atmospheric and Oceanic Sciences, University of Wisconsin—Madison, 1225 W. Dayton St., Madison, WI 53706.]
- Sutcliffe, R. C., and A. G. Forsdyke, 1950: The theory and use of upper air thickness patterns in forecasting. *Quart. J. Roy. Meteor. Soc.*, **76**, 189–217.
- Uccellini, L. W., 1990: Processes contributing to the rapid development of extratropical cyclones. *Extratropical Cyclones: The Erik Palmén Memorial Volume*, C. W. Newton and E. O. Holopainen, Eds., Amer. Meteor. Soc., 81–105.
- Whitaker, J. S., L. W. Uccellini, and K. F. Brill, 1988: A model-based diagnostic study of the rapid development phase of the Presidents’ Day cyclone. *Mon. Wea. Rev.*, **116**, 2327–2365.